Original Article

Institution of MECHANICAL ENGINEERS

Journal of AEROSPACE ENGINEERING

Proc IMechE Part G:
J Aerospace Engineering
0(0) 1–15

DOI: 10.1177/0954410013511596
uk.sagepub.com/jaero

SAGE

An integrated nonlinear model-based approach to gas turbine engine sensor fault diagnostics

Feng Lu[1,2], Yu Chen[1,3], Jinquan Huang[1], Dongdong Zhang[1,2] and Nan Liu[1]

Abstract

Aircraft engine sensor fault diagnosis is closely related technology that assists operators in managing the health of gas turbine engine assets. As all gas turbine engines will exhibit performance changes due to usage, the on-board engine model built up initially will no longer track the engine over the course of the engine's life, and then the model-based method for sensor fault diagnosis tends to be failure. This necessitates the study of the sensor fault diagnosis techniques due to usage over its operating life. Based on our recent results, an integrated approach based on nonlinear on-board model is developed for the gas turbine engine sensor fault diagnostics in this paper. The architecture is mainly composed of dual nonlinear engine models; one is a nonlinear real-time adaptive performance model and the other a nonlinear on-board baseline model. The extended Kalman filter estimator in the nonlinear real-time adaptive performance model is used to obtain the real-time estimates of component performance, and the nonlinear on-board baseline model with performance periodically update to provide the nominal reference in flight. The novel update strategy to sensor fault threshold based on the model errors and noise level is also presented. Important results are obtained on step fault and pulse fault behavior of the engine sensor. The proposed approach is easy to design and tune with long-term engine health degradation. Finally, experiment studies are provided to validate the benefit of the engine sensor fault diagnostics.

Keywords

Gas turbine engine, sensor fault diagnostics, health degradation, integrated nonlinear model, nonlinear filtering, threshold update

Date received: 8 May 2013; accepted: 10 October 2013

Introduction

In-flight sensor fault diagnosis is critical to maintaining aircraft engine operation reliably. The engine is operated at demanded conditions by the full authority digital electronic control (FADEC) system, which computes control commands based on sensor measurements.[1] Because most sensors for FADEC work in the harsh environment, high temperature, and strong vibration, they are easy to be failure, and any undetected sensor faults may result in an undesirable condition.[2,3] It is crucial to diagnose the sensor fault as soon as possible to avoid hazard scenarios, and an in-flight sensor fault diagnosis system with high reliability is essential to enhance flight safety.[4]

Sensor fault diagnostics for aircraft engine has received considerable attention and many works have been reported.[5–10] Wallhagen and Arpasi[11] proposed using analytical redundancy sensor technology to improve the reliability of the engine control system in 1974. Spang and Corley[12] discussed the fault indication and correction action system for sensor diagnosis, and then it is applied in the FADEC plan of T700, JTDE, and F404 but cannot detect soft failures. Merrill and coworkers[4,13] developed a detection, isolation, and accommodation program via analytical redundancy, and determined the minimum detectable levels of sensor failures for an F100 turbofan engine. NASA developed an analytical redundancy design for engine reliability improvement.[14,15] Bettocchi and

[1]College of Energy and Power Engineering, Nanjing University of Aeronautics and Astronautics, Nanjing, China
[2]Aviation Motor Control System Institute, Aviation Industry Corporation of China, Wuxi, China
[3]Guizhou Liyang Aero Engine Corporation, Guiyang, China

Corresponding author:
Jinquan Huang, College of Energy and Power Engineering, Nanjing University of Aeronautics and Astronautics, Nanjing, China.
Email: jhuang@nuaa.edu.cn

Spina[16] presented a method based on analytical redundancy techniques for sensor fault detection in gas turbines, and I/O linear models are used for residuals generation permitting the identification of possible sensor faults. The fault indices are usually the thresholds of amplitude and slope, and built-in-test technology is also used for sensor fault diagnosis in engineering. Simani et al.[17] designed an improved observer for sensor fault diagnosis for a power plant. Kobayashi[18] developed a fault detection and isolation (FDI) system that utilizes a bank of Kalman filters for aircraft engine sensor and actuator FDI in conjunction with the detection of component faults. The approaches to diagnose the sensor faults discussed above are mainly based on engine model, while the novel data-based ones rapidly developed with the intelligent computing methods emerging in large number in the past 20 years. Ogaji et al.[19] reported multiple-sensor fault-diagnoses for a two-shaft stationary gas turbine. Mattern et al.[20,21] presented the results of applying neural network to validate sensor on a simulation platform of a turbofan engine. Randal et al.[22] presented neural networks and multiple failures assumption methods for fault diagnosis of sensors and actuators. Zhernakov[23] described diagnostics and checking of gas-turbine engines parameters by hybrid expert systems. Aretakis et al.[24] discussed identification of sensor faults on turbofan engines using pattern recognition techniques.

In short, the research studies on aircraft engine sensor fault diagnosis mainly include the data-based methods and the model-based methods. The latter ones fulfill the functions via several types of aircraft engine model, such as linear model, nonlinear model, and so on. The on-board engine models are usually built up with aircraft engine component characteristics and pneumatic thermodynamic equations. There is no need of a priori knowledge of aircraft engine or sensor fault modes, being less sensitive to measurements than that of data-based approaches.[25–27] The main idea of model-based one is that the sensor falls to failure when the residual between the sensor measurement and the model output violates its threshold. The aircraft engine model is initially built up at a nominal condition, and there is no health degradation. Nevertheless, the real engine performance degrades with usage, and the on-board model does not track the sensed engine outputs over time.[28] Then, engine model cannot be always taken as the reference baseline during the whole lifetime, and the in-flight diagnostic systems will lose their effectiveness after the certain cycle numbers.

To address this issue, one method that the engine health condition is estimated off-line by steady-state data recorded during flight, and then used to update the health parameters of the on-board baseline model is discussed.[29–31] The shortcomings of the off-line estimate include the post-flight processing of a small number of the measurements collected each flight and only available in ground-station. Kobayashi and Simon[32,33] developed a baseline system and an enhanced system for aircraft engine on-line diagnostics, while they are focused on the dual-channel sensor measurements. References [34,35] present an enhanced on-board architecture for trend monitoring and gas path fault diagnosis and provide advanced on-board model-based estimation capabilities. The architecture contains real-time adaptive performance model (RTAPM) and performance baseline model (PBM), both of which are built up with piecewise-linear dynamic scheduled models. The linear model is derived from the engine component level model (CLM), linearization errors are introduced in the modeling process that will decrease the accuracy of performance estimation.[36,37] The linear Kalman filter (LKF) for health estimate is effective only within a limited linearized range, and the constant threshold tends to be failure to diagnose the sensor faults because of the model errors change over the engine lifetime.

For the reasons described above, an integrated approach that utilizes dual nonlinear on-board engine model is developed for aircraft engine in-flight sensor fault diagnostics, and the benefit of this integration is investigated in the experiments and analysis in this paper. The proposed integrated nonlinear architecture with the sensor fault diagnostic logic is applicable to diagnose aircraft engine sensor failures while the engine experiences continuously gradual degeneration over the course of the engine's life. The self-tuning real-time performance model, including the nonlinear engine model and the extended Kalman filter (EKF) filter, is referred to real-time performance estimation. A piecewise predictor is used to obtain the real-time performance update values for the baseline model. The baseline model, whose health parameters are updated with the soft update strategy, produces the sensor reference outputs on-line. The sensor fault threshold, used in the sensor fault diagnosis logic, is tuned with the model update. As a consequence, considering an aircraft engine is a complicated thermo-mechanical system and its performance degenerates with usage; this inevitably necessitates the employment of the fused model update mechanism from nonlinear systems theory to the engine sensor fault diagnosis. This paper is an attempt toward the above idea.

This paper is organized is as follows. In section "Turbofan engine model and health estimation," nonlinear aircraft engine model and its performance estimation approach are discussed; the integrated nonlinear architecture is developed, and then the nonlinear real-time adaptive performance model, nonlinear on-board baseline model (NBM), and the sensor fault diagnostic module are present in details in section "Nonlinear integrated architecture for sensor fault diagnosis." Section "Experiments and analysis" provides experiments and analysis for the

validation of the developed integrated nonlinear approach and the next section presents the discussion and analysis on the two-update strategy, and finally our work is summarized in the last section.

Turbofan engine model and health estimation

Turbofan engine nonlinear model

A high bypass ratio turbofan engine is depicted in Figure 1. The airflow is driven into the fan after through an inlet. Air is separated into two streams before the compressor: one stream passes through the annular bypass duct and then leaves the engine core, and the other one through the engine core. The air through the core moves ordinal through booster and high-pressure compressor (HPC). Fuel is sprayed into the combustor, mixed with air, and burned to produce hot gas to drive the turbines. There are two rotating shafts, through which the high-pressure turbine (HPT) drives the HPC and the low-pressure turbine (LPT) drives both the fan and the booster. The gas leaves the LPT and then is guided into the nozzle, and it has a variable throttle area.

The turbofan engine mathematical model studied includes several individual components, denoted as CLM, and each component requires input thermodynamics variables and produces corresponding outlet variables. The model consists of mathematical equations, characteristic maps, operating parameter tables, etc., which describes the thermodynamic relationships of various variables for each component. The turbofan engine CLM is built up with the following assumption, no combustion delay, the component characteristics unchanged with the Reynolds number, and zero-dimension flow. The component thermodynamic variables in cross-sections, such as total pressure, the total temperature, efficiency, and flow capacity, can be computed as in ref.[38–40] The common operations of the turbofan engine CLM that follow flow capacity balance are expressed as follows:

$$\begin{cases} W_{22} - W_{21} = 0 \\ W_{24} - W_{23} = 0 \\ W_{41} - W_{Acool} - W_{Bcool} - W_4 = 0 \\ W_{42} - W_{41} = 0 \\ W_9 - W_5 = 0 \\ W_{19} - W_{16} = 0 \end{cases} \tag{1}$$

The acronyms of the equation above are detailed in Table 1. Overall characteristic maps are used to represent the performance of rotary component which are good enough for real-time simulation. The map value of corrected flow capacity $W_{i,cor}$ and efficiency SE_i for each component are computed from bivariate functions of the component pressure ratio π_i, and the component corrected speed $n_{i,cor}$ as follows:

$$\begin{aligned} W_{i,cor} &= f_{W,i}(\pi_i, n_{i,cor}) \\ SE_i &= f_{SE,i}(\pi_i, n_{i,cor}) \\ n_{i,cor} &= n_i / n_{i,d} \Big/ \sqrt{(T_i/T_{i,d})} \\ W_i &= W_{i,cor}(P_i/P_{i,d}) \Big/ \sqrt{(T_i/T_{i,d})} \end{aligned} \tag{2}$$

where the subscript d means the design point and i represents corresponding rotary component. The flow capacity balance equations are implicit functions of the pressure ratios $\pi_{Ft}, \pi_{Fr}, \pi_B, \pi_C, \pi_{HT}, \pi_{LT}$ and can be represented as the following six equations:

$$g_j(\pi_{Ft}, \pi_{Fr}, \pi_B, \pi_C, \pi_{HT}, \pi_{LT}) = 0 \quad j = 1, 2, \ldots, 6 \tag{3}$$

The engine CLM in dynamics must also account for the effects of rotor inertia, which are used to calculate the flow capacities in cross-sections with the component performance map and the six guess variables,

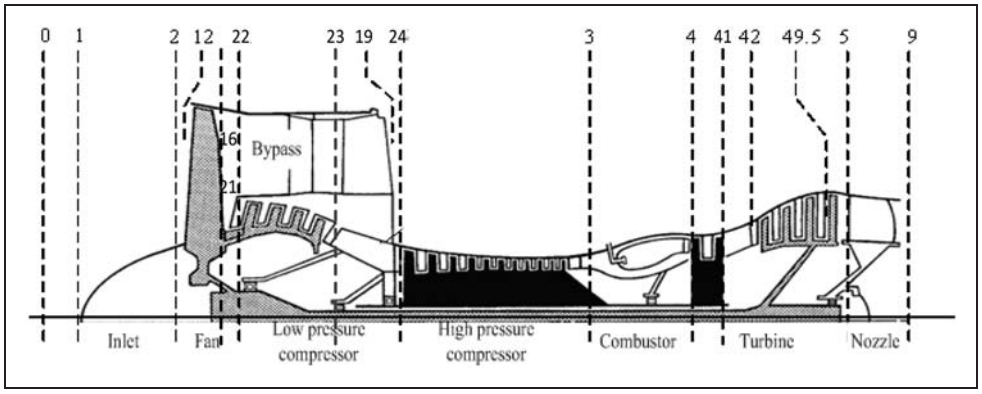

Figure 1. Diagrammatic sketch of a high bypass ratio turbofan engine.

Table 1. Turbofan engine CLM thermodynamic parameters.

Acronyms	Augment state	Acronyms	Augment state
W_{21}	Fan outlet to the core duct flow capacity	N_{HT}	Power produced by the HPT
W_{22}	Booster inlet flow capacity	N_{LT}	Power produced by the LPT
W_{23}	Booster outlet flow capacity	N_C	Power used for the HPC
W_{24}	HPC inlet flow capacity	N_T	Power used for the accessories
W_4	Combustor outlet flow capacity	N_B	Power used for the booster
W_{41}	HPT outlet flow capacity	N_F	Power used for the fan
W_{42}	LPT inlet flow capacity	π_{Ft}	Fan blade tip pressure ratio
W_5	LPT outlet flow capacity	π_{Fr}	Fan blade root pressure ratio
W_9	Nozzle core duct outlet flow capacity	π_B	Booster pressure ratio
W_{16}	Fan bypass duct outlet flow capacity	π_C	HPC pressure ratio
W_{19}	Nozzle bypass duct outlet flow capacity	π_{HT}	HPT pressure ratio
W_{Acool}	Flow capacity to cool the turbine inlet guide vane	π_{LT}	LPT pressure ratio
W_{Bcool}	Flow capacity to cool the turbine blade tip	J_H	High-pressure spool inertia
η_{Hspool}	High-pressure spool efficiency	J_L	Low-pressure spool inertia
η_{Lspool}	Low-pressure spool efficiency		

CLM: component level model; HPC: high-pressure compressor; LPT: low-pressure turbine; HPT: high-pressure turbine.

$\pi_{Ft}, \pi_{Fr}, \pi_B, \pi_C, \pi_{HT}, \pi_{LT}$. The current shaft speeds, n_L, n_H, are computed via the last step speeds and the shaft accelerations from equation (4).

$$\begin{cases} \left(\frac{30}{\pi}\right)^2 \frac{1}{J_H n_H}\left[N_{HT}\eta_{Hspool} - N_C - N_T\right] = \frac{\mathrm{d}n_H}{\mathrm{d}t} \\ \left(\frac{30}{\pi}\right)^2 \frac{1}{J_L n_L}\left[N_{LT}\eta_{Lspool} - N_F - N_B\right] = \frac{\mathrm{d}n_L}{\mathrm{d}t} \end{cases} \tag{4}$$

The common operating expressions of the turbofan engine CLM follow the flow capacity balance as same as the dynamic ones in equation (1) and the two shaft acceleration $\dot{n}_L, \dot{n}_H$ equal zero in steady state. Then, the spool power balance is satisfied and equation (4) can be written as follows:

$$\begin{cases} N_{HT}\eta_{Hspool} - N_C - N_T = 0 \\ N_{LT}\eta_{Lspool} - N_F - N_B = 0 \end{cases} \tag{5}$$

There are eight guess variables, π_{Ft}, π_{Fr}, π_B, π_C, π_{HT}, π_{LT}, n_L, n_H, for the engine CLM in steady state, and its operating equations can be represented as the following nonlinear expression:

$$g_j(n_L, n_H, \pi_{Ft}, \pi_{Fr}, \pi_B, \pi_C, \pi_{HT}, \pi_{LT}) = 0, \quad j = 1, 2, \ldots, 8 \tag{6}$$

Both the common operating equations of the steady state (equation (4)) and the dynamics (equation (6)) are solved via the Newton–Raphson method, and iterative process for the roots in each step stops once one of the following conditions is satisfied: the iteration error no more than 0.001 or the maximum iteration number to 40. The rotating component efficiency, SE, and flow capacity, W, are usually used to indicate turbofan engine gas path performance, and their deteriorated valves are denoted as health parameters.

$$\begin{aligned} \Delta SE_i &= \frac{SE_i}{SE_{i,r}} - 1 \quad i = 1, 2, 3, 4 \\ \Delta SW_j &= \frac{W_j}{W_{j,r}} - 1 \quad j = 1, 2, 3 \end{aligned} \tag{7}$$

where the subscript r means to the operating point. There are seven health parameters of rotor components considered in this paper: fan efficiency ΔSE_1, fan flow capacity ΔSW_1, HPC efficiency ΔSE_2, HPC flow capacity ΔSW_2, HPT efficiency ΔSE_3, HPT flow capacity ΔSW_3, and HPT efficiency ΔSE_4. The health parameter equals 0 when the component operates with no degeneration in initial cycle number.

The turbofan engine CLM is programmed by C language and packaged with dynamic link library (DLL) for calling in MATLAB environment.[41–43] The DLL of the engine CLM runs the steady state at the first step and then runs dynamics. The function outputs in DLL are the measurements y, and the inputs consist of flight condition c, control variables u, and health parameters Δh. The speeds are used to the state vector x conventionally, and the health parameters Δh are augmented into the state vector in the nonlinear model here, denoted as $x_{aug,k}$.[38,42,43] Then, the discretized time invariant nonlinear model of the turbofan engine from the CLM can be summarized as follows:

$$\begin{aligned} x_{aug,k+1} &= \begin{pmatrix} x_{k+1} \\ \Delta h_{k+1} \end{pmatrix} = \begin{pmatrix} f(x_k, \Delta h_k, u_k, c_{ond}) \\ \Delta h_k \end{pmatrix} + \begin{pmatrix} w_k \\ n_k \end{pmatrix} \\ y_k &= h(x_k, \Delta h_k, u_k) + v_k \end{aligned} \tag{8}$$

where $u = [Wf, A_8]^T$ is the two-element control vector, $x = [n_L, n_H]^T$ the two-element state vector, $\Delta h = [\Delta SE_1, \Delta SW_1, \Delta SE_2, \Delta SW_2, \Delta SE_3, \Delta SW_3, \Delta SE_4]^T$, and $c = [H, Ma]^T$ the two-element environmental vector. $\{w_k\}$ and $\{n_k\}$ are separately the process noise sequences, $\{v_k\}$ is the measurement noise sequences, and they are uncorrelated zero mean Gaussian noises.

Engine model health parameters estimate

To prevent the engine model deficiencies from being absorbed into the tuners (efficiencies, flow capacities, etc.), it is necessary to create an engine model to track the engine performance changes with enough accurate. As depicted in equation (8), the health parameters augmented into the model state vector is an effective way to improve the accurate model over its lifetime. The LKF is used to estimate the health parameters in the state vector model, and it makes the engine model match much better the sensed outputs by tuning the health parameters.[5,31–35]

The LKF is designed to off-line linearize the nonlinear system around a nominal state trajectory. The errors are inevitably brought in the model linearization process, and it will directly influence the estimation accuracy. Two nonlinear state estimation algorithms, the unscented Kalman filter (UKF) and the EKF, then emerged and are used in the aircraft engine application.[33,36,37] Kobayashi and Simon[33] have indicated that the aircraft engine nonlinearities are mild enough so that the UKF does not provide much better performance than the EKF but have more computational effort. Therefore, the EKF is selected to estimate the augmented state vector in the nonlinear system of equation (8). Taylor series is used to expand the nonlinear model around the operating point. We assume that the following standard conditions are satisfied.

$$\begin{aligned} E\left[x_{aug,0}\right] &= \bar{x}_{aug,0} \\ E\left[w_{aug,k}\right] &= 0 \\ E[v_k] &= 0 \\ E\left[\left(x_{aug,0} - \bar{x}_{aug,0}\right)\left(x_{aug,0} - \bar{x}_{aug,0}\right)^T\right] &= P_0^+ \\ E\left[w_{aug,k} w_{aug,m}^k\right] &= Q\delta_{km} \\ E\left[v_k v_m^k\right] &= R\delta_{km} \\ E\left[w_{aug,k} v_m^k\right] &= 0 \end{aligned} \tag{9}$$

where $E[\,]$ is the expect operator in the statistics. The delta function δ_{km} equals 1 when $k = m$, otherwise to 0. The matrices P, Q, and R are the covariance of state errors, process noise, and measurement noise, respectively. Assume that the control is known so that $\Delta u_k = 0$. The EKF for the nonlinear engine model starts with the following time update equations.

$$\begin{aligned} P_k &= FP_{k-1}^+ F^T + Q \\ \hat{x}_{aug,k} &= f\left(\hat{x}_{k-1}^+, \hat{h}_{k-1}^+, u_{k-1}\right) \end{aligned} \tag{10}$$

where the Jacobian F in the preceding equation is given as

$$F = \frac{\partial f\left(\hat{x}_{k-1}^+, \hat{h}_{k-1}^+, u_{k-1}\right)}{\partial x_{aug}} \tag{11}$$

Then the EKF performs the following measurement update equations:

$$\begin{aligned} K_k &= P_k H^T \left(HP_k H^T + R\right)^{-1} \\ \hat{x}_{aug,k}^+ &= \hat{x}_{aug,k} + K_k\left[y_k - h\left(\hat{x}_{aug,k}\right)\right] \\ P_k^+ &= (I - K_k H)P_k \end{aligned} \tag{12}$$

where the Jacobian H in the measurement equation is given as

$$H = \frac{\partial h\left(\hat{x}_{aug,k}\right)}{\partial x_{aug}} \tag{13}$$

Nonlinear integrated architecture for sensor fault diagnosis

A linear integrated architecture for trend monitoring and gas-path diagnostics is discussed in Refs[34,35], and in the architecture aircraft engine linear model is taken as the performance baseline, and the LKF estimator is used for health estimate. As known in Ref.[36], the EKF outperforms the LKF on health parameter estimate for gas turbine engine, and therefore the integrated architecture based on the nonlinear model and the EKF estimator is introduced to aircraft engine sensor fault diagnostics in-flight during the engine whole lifetime. The strategies of model update and sensor fault threshold update for the integrated approach are improved and designed in this paper.

An overview of the integrated nonlinear architecture is present in Figure 2. The architecture includes two on-board real-time nonlinear engine models operating in parallel and one sensor fault diagnostic module. The first engine model, referred to as the nonlinear real-time adaptive performance model (NRAPM), implements an EKF estimator to provide real-time unmeasured performance estimates for tracking engine component performance during the engine health degradation. The second model, referred to as the independent nonlinear baseline model (NBM), utilizes in-flight health parameter estimates to produce the reference of sensed measurements for sensor fault diagnostics. The sensor fault

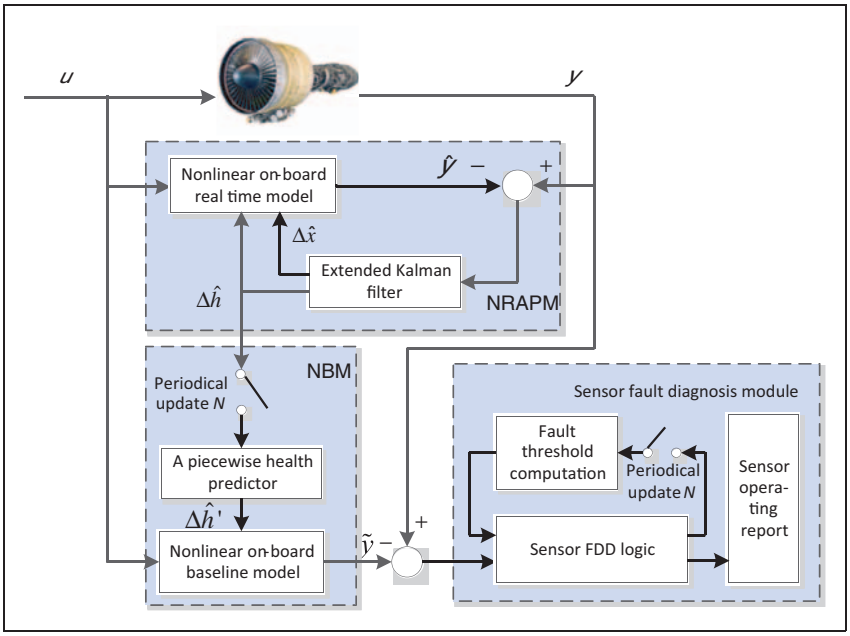

Figure 2. An integrated nonlinear architecture for turbofan engine sensor fault diagnostics.
NRAPM: nonlinear real-time adaptive performance model; NBM: nonlinear on-board baseline model.

diagnosis module implements sensor fault threshold periodical update, and the sensor operating report is obtained by the sensor FDD logic. The detailed modules in the architecture are described in the following section.

Nonlinear real-time adaptive performance model

The purpose of the NRAPM is to provide a continuous assessment of aircraft engine health condition. It consists of a nonlinear on-board real-time model and an associated tracking filter that on-line tunes the model track the performance changes of the physical engine by the feedback sensed measurements. Health parameters are used as a measure of engine health degradation and reflect the effects of performance deterioration on sensed engine variables. The EKF is applied to capture gradual engine performance deterioration and produces real-time estimates of the engine's augment state variables $\hat{x}_{aug}$. The EKF estimator receives the residuals between the sensed measurements and the engine model outputs to estimate the variables $\hat{x}_{aug}$, including the state variable $\hat{x}$ and health parameters $\Delta\hat{h}$, which are provided as inputs to the nonlinear on-board real-time model. This process allows the model-produced estimates $\hat{y}$ to track the sensed measurements throughout, no matter whether the sensed values are actual engine outputs.

Nonlinear on-board baseline model

The NBM incorporates an independent version of the same nonlinear on-board engine model, and the inputs of the NBM mainly include the commands u and the estimated health parameters $\Delta\hat{h}$ in the NBM. When the NBM runs on-board, it continuously accepts commands u, flight condition c, and periodically updated health parameter estimates $\Delta\hat{h}$. The initial state variable x in the NBM is calculated by the corrected control variable u with the interpolation map. The periodic update of the health parameters allows the NBM adapt to normal performance deterioration that occurs gradually over time. Aircraft engine health degradation is only assumed to be gradual in the architecture. The NBM provides a baseline to the sensed measurements within the recent operating cycle.

A piecewise performance predictor which is applied to capture dynamics periodically updated the NBM health parameters to incorporate the effects of engine health degradation, and the estimated health parameters from the NRAPM are flowed into the predictor by the performance update switch. As sensor faults are expected to manifest themselves as sudden shifts, the real-time health parameter estimates generated by the NRAPM's EKF will immediately absorb sensor faults. Nevertheless, the health parameters employed by the NBM are updated only periodically, and the sensor fault will not be reflected in the health parameter inputs to the NBM, resulting in a measurable divergence of actual sensor values from respective NBM estimates.

The health parameters $\Delta\hat{h}'$ used for the nonlinear on-board baseline model in the NBM come from a piecewise performance predictor but not directly from the periodic health parameters $\Delta\hat{h}$. Therefore, the frequency of the periodic health parameters $\Delta\hat{h}$ update from the NRAPM is user-specified but is typically not needed to be once per flight as in Ref.[31] As we know that the health parameters can be

updated every N cycle, and before the next update the health parameters are constant, the differences between the NBM and the real engine will increase with the use. Shortening the update period is one way to decrease the model errors; however, it will observably result in the manual, material, and cost consuming. Therefore, a new strategy to update health parameters called soft update strategy is discussed. Assume that the update period is N, and the piecewise performance predictor in the NBM is as follows.

$$h'(n) = \begin{cases} h(0) & n < N \\ \dfrac{h(N) - h(0)}{N} n + h(0) & N \leqslant n < 2N \\ f(n) & n \geqslant 2N \end{cases} \quad (14)$$

From equation (14), we can see that the NBM health parameters $\Delta h'$ are initialized to the periodic health parameter $\Delta\hat{h}(0)$ from the NRAPM when the cycle number is less than N, and then the parameters $\Delta h'$ satisfy the linear function passing through the following two points $(0, \Delta h(0))$,$(N, \Delta h(N))$, and after the second update period $2N$ it can be fitted with the function $f(\cdot)$. Engine components will be consumed over thousands of repeated operating cycles while being subjected to a broad range of operating loads and conditions, including extreme temperature environments.[35] Weighting the pros and cons of the sensor fault diagnostic accuracy and the operating costs, the health parameters used for the NBM are updated each cycle by equation (14), and it is so-called piecewise performance predictor of the soft update strategy.

The health parameter deterioration of the gas path component in aircraft engine usually follows the quadratic function with the cycle number;[31] therefore, the function $f(\cdot)$ is assumed as the quadratic function that is followed with the series of periodical estimated health parameter $\Delta h(kT),\ k = 0, \ldots, K$.

Sensor fault diagnostics module

The estimated NBM outputs $\hat{y}$ and the sensed engine measurements y are designed to be used by a fault detection and diagnostic (FDD) logic for the sensor fault diagnosis on-line in sensor fault diagnostic module. As discussed in Ref.,[27] the keys to the model-based sensor fault diagnosis are the baseline model accuracy and sensor fault threshold selection. The former has been discussed in section "Nonlinear on-board baseline model," and we propose the periodical update to compute fault threshold for the latter in this section. The threshold is determined by the statistical characteristics of sensor measurement noises and the model errors. The engine variable measured by sensor is expressed as follows:

$$y_k = \tilde{y}_k + \Delta y_k + v_k \quad (15)$$

The parameters $\tilde{y}_k$ and Δy_k separately represent the engine sensed measurement and the modeling error. The parameter v_k is the zero mean, normally distributed white noise that corrupts the measurements, denoted as $v_k \sim N(0,\sigma^2)$. For each measured parameter, the analytical residual is defined as follows:

$$r^i = \frac{|y^i - \tilde{y}^i|}{\sigma_i} = \frac{|v + \Delta y|}{\sigma_i} \quad (16)$$

where σ_i indicates the standard deviation of the ith sensor measurement uncertainty. The NBM generates the expected output values under the condition without any sensor faults. The analytical residual computed for each sensor is compared against the threshold $\tau^n{}_i$ at the nth cycle. If an analytical residual r^i exceeds a threshold $\tau^n{}_i$, it indicates the existence of an anomaly and the ith sensor fault.

Considering the random variable v_k/σ follows the standard normal distribution, and 3σ criterion, the threshold $\tau^n{}_i$ can be calculated by the following equation:

$$\tau_i^n = \left|\frac{\Delta y}{\sigma_i}\right| + 3 \quad (17)$$

As previously mentioned, engine performance is generally deteriorated, and then the modeling errors will be changed with usage. Therefore, the sensor fault thresholds need to be updated periodically with the baseline model errors. The threshold update rate is the same as the health parameter update frequency, equaling to N.

Experiments and analysis

The experiments are carried out in the hardware-in-loop (HIL) system, and the sensor fault diagnosis approach proposed above is designed and downloaded into the NI CompactRIO (cRIO), high-performance programmable automation controller (PCA) hardware. The NI cRIO-9024 and the NI cRIO 9014 are used to build up the cRIO PCA. The NI cRIO-9024 embedded real-time controller features an industrial 800 MHz real-time Freescale processor for deterministic, reliable real-time applications and contains 512 MB of DDR2 RAM and 4 GB of non-volatile storage for holding programs and logging data. In the HIL system, the turbofan engine CLM has taken the place of the actual engine, and it experiences the gradual deterioration in order to represent the aircraft engine used in the real environment. The NI cRIO-9014 eight-slot, reconfigurable embedded chassis is part of the cRIO PCA platform. The engine CLM balances flow capacity (power) equations of the system are calculated at a rate of 200 Hz, and the sampling frequency used for the nonlinear model sensor fault diagnostics is 50 Hz. The EKF estimates

health parameters and tracks the engine health condition at each sample point. The covariances of process noise and measurement noise are separately obtained from the standard deviation in Tables 2 and 3. Sensor dynamics are assumed to be of high enough bandwidth that they can be ignored in the dynamic equations.

Considering the engine works at the cruise in the most time, the experiments of sensor fault diagnosis for the engine are carried out at this operating point, and the referred parameters can be seen in Tables 2 and 3. The proposed approach based on nonlinear integrated model is evaluated to the capability of sensor fault diagnostics in flight over the course of lifetime.

Health parameter estimate over the lifetime

Engine component performance gradual deteriorations are injected into all seven turbofan engine health parameters. The deterioration profile that the engine model will undergo is starting from initial normal condition, then drifting following quadratic function, and at the end of the sequence (6000 cycle number) the health parameters is as follows: −2.85% on *SE1*, −3.65% on *SW*1, −9.4% on *SE*2, −14.1% on *SW*2, −3.81% on *SE*3, 2.57% on *SW*3, and −1.08% on *SE*4. The deterioration profile specifies a unique health condition at each sample point. Every 400 cycle number the health parameters are stored and updated both for the predictor model during the whole 6000 cycles, and the estimated parameters are on-line generated by the state estimators.

Figure 3 shows the responses to 2% fan speed (n_L) sensor step fault both on the NRAPM and the NBM at the 3000 cycle number. The estimated value via the NRAPM tracked the sensor n_L value well (in Figure 3(a)) with the health parameters real-time tuning (in Figure 3(b)). If the NRAPM is taken as the reference baseline, we cannot obtain 2% sensor n_L step fault, and at the same time the estimated health parameters cannot reflect the engine actual health status. The 2% sensor n_L step fault is represented in Figure 3(c) by the residuals between the n_L estimated value via the NBM and the actual sensed one.

As can be seen from Figure 3, the NRAPM outputs are able to track the sensed engine values closely,

Table 2. Turbofan engine CLM health parameter, operating point, standard deviation and degeneration maximum.

Augment state	Acronyms	Operating point	Standard deviation	Deteriorate maximum (%)
Fan efficiency	SE_1	1	0.0005	−2.85
Fan airflow capacity	SW_1	1	0.0005	−3.65
HPC efficiency	SE_2	1	0.0005	−9.4
HPC airflow capacity	SW_2	1	0.0005	−14.1
HPT efficiency	SE_3	1	0.0005	−3.81
HPT airflow capacity	SW_3	1	0.0005	2.57
LPT efficiency	SE_4	1	0.0005	−1.08

CLM: component level model; HPC: high-pressure compressor; LPT: low-pressure turbine; HPT: high-pressure turbine.

Table 3. Turbofan engine CLM measurements at the cruise.

Variables	Acronyms	Operating point	Standard deviation
Fuel flow	Wf	2.5 kg/s	
Variable nozzle area	A_8	0.54 m^2	
Low-pressure rotor speed	n_L	3799 r/min	0.0015
High-pressure rotor speed	n_H	11341 r/min	0.0015
Fan exit pressure	P_{13}	175677 Pa	0.0015
HPC inlet pressure	P_{25}	321039 Pa	0.0015
HPC inlet temperature	T_{25}	698 K	0.002
HPC exit pressure	P_3	3266005 Pa	0.0015
HPC exit temperature	T_3	1122 K	0.002
LPT exit pressure	P_5	181377 Pa	0.0015
LPT exit temperature	T_5	1053 K	0.002

CLM: component level model; HPC: high-pressure compressor; LPT: low-pressure turbine; HPT: high-pressure turbine.

and the post-fault residuals between the on-board model and actual engine are minimal since the EKF provides continuous tuning to the health parameters; therefore, the NRAPM cannot be taken as the baseline for sensor fault diagnosis purpose alone. Conversely, the health parameters for the NBM are held constant before the one cycle over no matter whether the sensor fault happens. The residuals between the NBM estimated value and the sensed one are clearly discernible, which can be used for sensor fault diagnostics. The key difference of the two on-board nonlinear models is the health parameters update strategy.

Sensor fault threshold update

The conventional in-flight sensor fault diagnosis system will eventually lose its effectiveness as the engine is normally deteriorated over time. This happens because the baseline model output values will not reflect the sensed engine ones. To keep the capability of sensor fault diagnostics within the lifetime, the health parameters of the NBM must be updated. This soft update is completed by the following two processes of feeding the estimated health condition values: the piecewise predictor model periodical update from the variables Δh and the NBM performance real-time update with the variables $\Delta h'$. The estimates of sensor n_L, P_3, and T_5 by the two on-board baseline models with different update strategies are represented in Figure 4, where the gas turbine engine is subject to the specific health deterioration profile over its lifetime of 6000 cycles discussed in section "Health parameter estimate over the lifetime." The physical parameters y in the following figures have been normalized.

In the experiment, the health status of the baseline is updated each 400 cycle numbers. In Figure 4, the black line denotes the engine actual sensed value, the red line denotes the output of nonlinear baseline model with no update (marked I), the blue line denotes the output of linear baseline model with periodical update (marked II), and the pink line denotes the output of the nonlinear baseline model with the soft update strategy (marked III). As can be seen from Figure 4, if the baseline is not updated from the nominal condition, the residuals between the baseline values and the actual sensed measurements will increase with the operational cycle number. The on-board performance baselines, updated by the two update approaches, produced the outputs that could track the engine actual sensed values. Compared with the PBM, the NBM has less estimated errors to the actual performance changes.

As discussed in section "Sensor fault diagnostics module," the threshold of the analytic residual is determined not only by the measurement noise but also by the modeling error. After we have obtained the modeling errors at the cruise, the analytic threshold for each sensor can be computed as equation (17). Table 4 shows the computational results of modeling errors and thresholds at the 3000 cycle number and the 4200 cycle number for the three baselines. As can be seen from Table 4, the modeling error of sensor n_L by the III at the 3000 cycle number equals -0.06, provided the standard deviation of sensor n_L measurement noise equals 0.15% in Table 3, then the fault threshold of the sensor can be calculated to 3.40. We can see that the threshold decreases with the absolute of the modeling error, and the updated nonlinear model is corresponding to the smallest threshold.

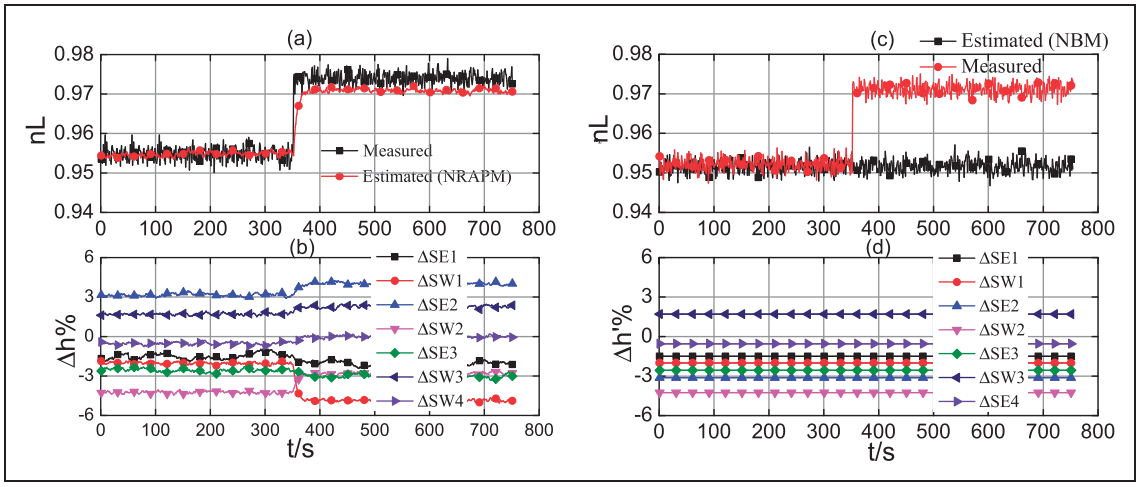

Figure 3. Comparison of the NRAPM and the NBM responses to 2% sensor n_L step fault at the 3000 cycle number: (a) sensor n_L estimates by the NRAPM; (b) performance estimates Δh by the NRAPM; (c) sensor n_L estimates by the NBM; and (d) outputs of the piecewise performance predictor $\Delta h'$ for the NBM.
NRAPM: nonlinear real-time adaptive performance model; NBM: nonlinear on-board baseline model.

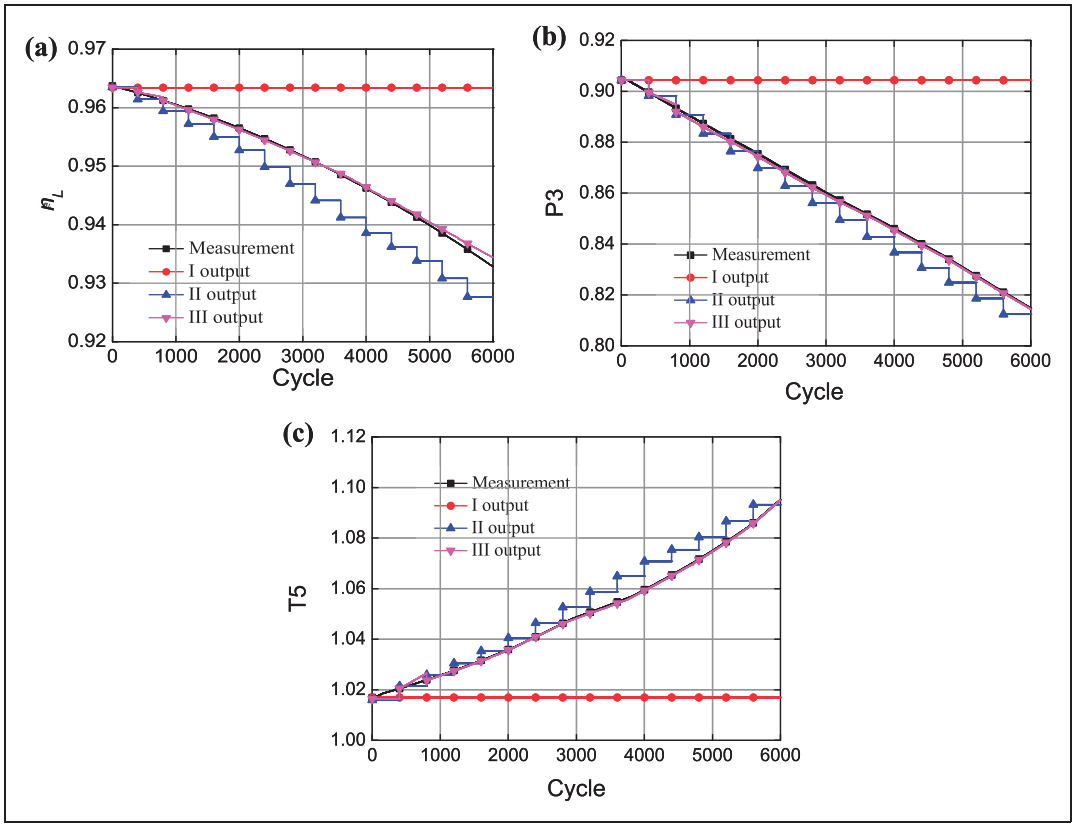

Figure 4. The baseline model output values with the performance deterioration over time: (a) n_L; (b) P_3; and (c) T_5.

Table 4. Gas turbine engine sensor fault thresholds.

	n_L at the 3000 cycle			T_{25} at the 4200 cycle		
	I	II	III	I	II	III
Modeling errors Δy (%)	−1.13	0.52	−0.06	0.70	−0.84	0.34
Threshold τ^n_i	10.53	6.47	3.40	6.50	7.20	4.70

Sensor fault diagnostics in flight

In order to verify the capability of the nonlinear integrated model-based approach to diagnose sensor faults, experiments on three fault diagnostics structures with step fault and pulse fault to sensed outputs are carried out. The structures are as follows: nonlinear approach without any update, the linear approach with periodical baseline update,[35] and the nonlinear approach with periodical baseline and threshold update.

The magnitude of 1%, 2%, and 5% step fault was separately injected into the sensor n_L at 10 s of the 3000 cycle number at the cruise as shown in Figure 5(a). The sensor n_L fault thresholds at the 3000 cycle number by the three approach have been calculated in Table 4, which are 10.53, 6.47, and 3.40 as depicted in Figure 5(b)–(d), respectively. The analytic residuals r_{nL} by the nonlinear without update are not exceeding its threshold $\boldsymbol{\tau}^{\mathbf{3000}}{}_{nL}$ under 1% and 2% step faults at 10 s, except 5% step faults in Figure 5(b). As can be seen from Figure 5(c) and (d), the analytic residuals grow obviously at 10 s, and all of them violate their thresholds under three step faults with three magnitudes. According to the above results, we can see that both the linear approach with model update and the nonlinear approach with model and threshold update could be used to discriminate the sensor n_L step fault at the 3000 cycle number, while the approach with no update is only effective to large magnitude step fault.

The results of the sensor n_L with a pulse fault are illustrated in Figure 6. As shown in Figure 6(b), the r_{nL} grows higher than the threshold $\boldsymbol{\tau}^{\mathbf{3000}}{}_{nL}$ when the fault magnitude is 5%. However, the r_{nL} value is only bigger than the threshold in part when the downward pulse with 1% or 2% magnitude, thus the upward pulse with 1% or 2% magnitude is undetectable at the 3000 cycle number through the nonlinear approach without update. The r_{nL} value is below its threshold $\boldsymbol{\tau}^{\mathbf{3000}}{}_{nL}$ as upward pulse with 1% magnitude,

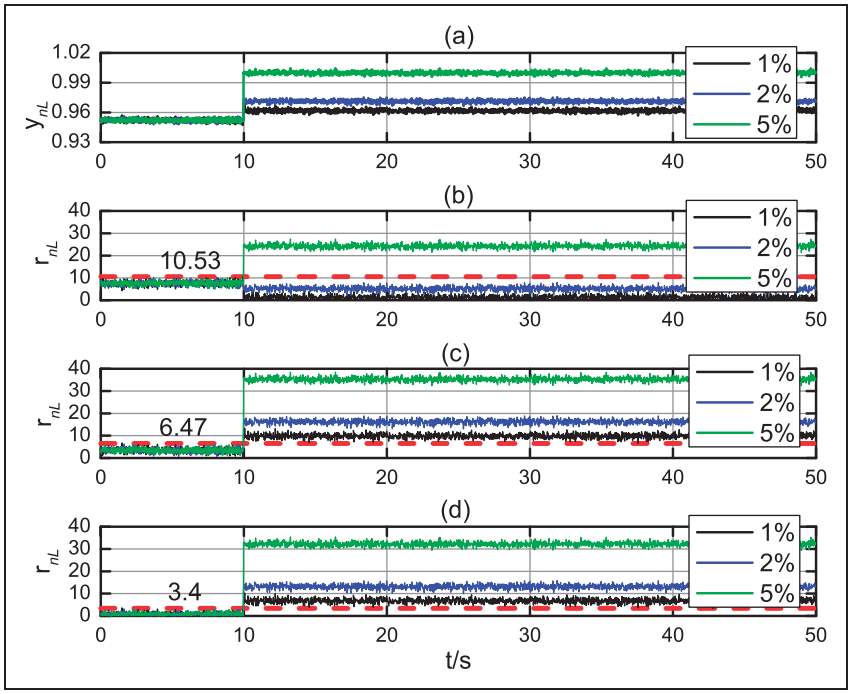

Figure 5. Comparison of the sensor n_L step faults at the 3000 cycle number: (a) signal of sensor n_L with step faults; (b) nonlinear approach without any update; (c) the linear approach with periodical baseline update; and (d) the nonlinear approach with both of baseline and threshold periodical update.

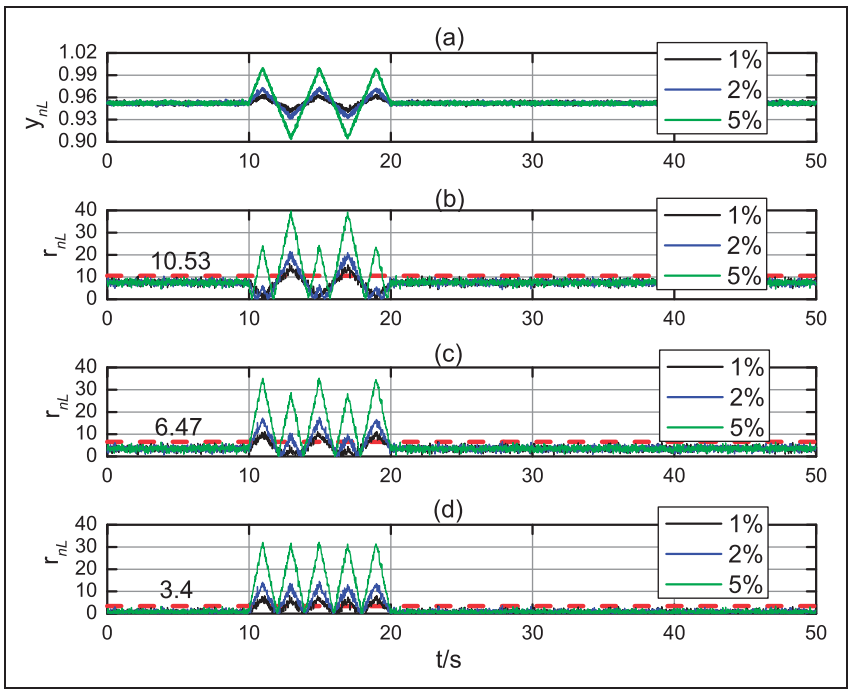

Figure 6. Comparison of the sensor pulse faults at the 3000 cycle number: (a) signal of sensor n_L with pulse faults; (b) nonlinear approach without any update; (c) the linear approach with periodical baseline update; and (d) the nonlinear approach with both of baseline and threshold periodical update.

while analytic residuals under the remaining magnitude violate their threshold by the linear approach with model update in Figure 6(c). Each residual exceeds its threshold no matter what magnitude and direction pulse fault in Figure 6(d), and it is consistent with the truth and the no misdiagnosis is produced by the proposed nonlinear integrated model-based approach.

From the experiment to the sensor n_L above, it seems that compared with the model update

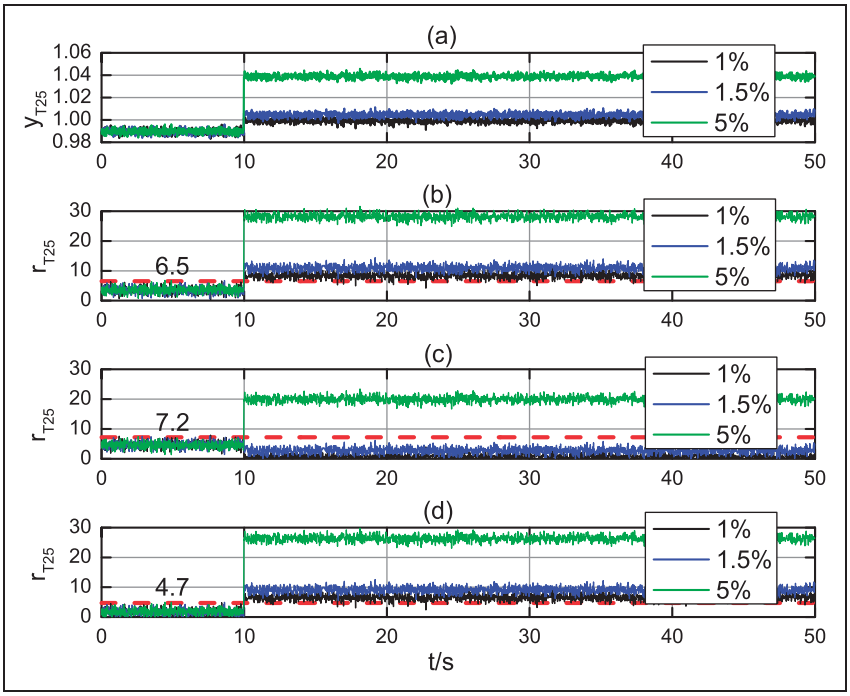

Figure 7. Comparison of the sensor T_{25} step faults at the 4200 cycle number: (a) signal of sensor T_{25} with step faults; (b) nonlinear approach without any update; (c) the linear approach with periodical baseline update; and (d) the nonlinear approach with both of baseline and threshold periodical update.

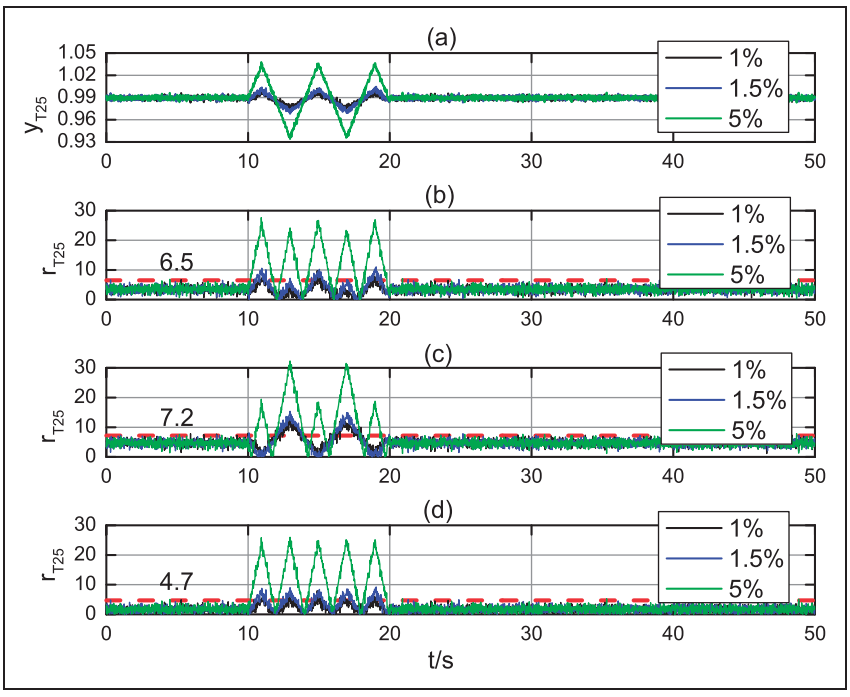

Figure 8. Comparison of the sensor T_{25} pulse faults at the 4200 cycle number: (a) signal of sensor T_{25} with pulse faults; (b) nonlinear approach without any update; (c) the linear approach with periodical baseline update; and (d) the nonlinear approach with both of baseline and threshold periodical update.

approach, the misdiagnosis is much easier to happen by the one without update. And it is true in the most scenarios except to the sensor T_{25} through the experiments. The results of the sensor T_{25} with step fault and pulse fault at the 4200 cycle number are described in Figures 7 and 8, respectively. The magnitudes of the sensor fault are 1%, 1.5%, and 5%, and the sensor T_{25} fault threshold at the 4200 cycle number can be referred to the Table 3. As shown in Figure 7(c), the analytic residuals r_{T25} are still below the

Table 5. Sensor fault diagnostic results under the sensor step fault at the 200 cycle number, at the 3000 cycle number, and at the 5800 cycle number.

		n_L	n_H	P_{13}	T_{25}	P_{25}	T_3	P_3	T_5	P_5
200 cycle number	IV	✓	✓	✓	✓	✓	✓	✓	✓	✓
	V	✓	✓	✓	✓	✓	✓	✓	✓	✓
3000 cycle number	IV	✓	✓	✓	✗	✓	✓	✓	✓	✓
	V	✓	✓	✓	✓	✓	✓	✓	✓	✓
5800 cycle number	IV	✗	✓	✗	✗	✓	✗	✓	✓	✓
	V	✓	✓	✓	✓	✓	✓	✓	✓	✓

threshold τ^{4200}_{T25} after the step fault with the magnitude 1% and 1.5% happens at 10 s, thus the linear approach with model update fails in these scenarios. However, the other two methods do well in three magnitudes of step fault. The pulse fault with the magnitude 1.5% and 5% can be detected by the nonlinear approach without update, but it does nothing to the downward pulse fault with magnitude 1% in Figure 8(b). The linear approach with model update loses its sensor fault detection ability to the upward pulse fault with both magnitude 1% and 1.5%. The proposed nonlinear approach maintains its effective capability to the all three pulse faults.

Table 5 shows the sensor fault diagnostic results to the scenario of each sensor 2% step fault at the 200 cycle number, the 3000 cycle number, and the 5800 cycle number of the whole lifetime by the conventional linear approach with model update (denoted as IV) and the proposed approach (denoted as V). Both of these two methods could diagnose all nine sensors well at 200 cycle number, while sensor T_{25} is misdiagnosed by the IV at the 3000 cycle number. With the use of the engine, the baseline model errors will increase. From Table 5, we can see that there are four sensor misdiagnose (n_L, P_{13}, T_{25}, and T_3) happening by the IV at the 5800 cycle number, while the proposed approach still has satisfactory diagnostic effectiveness.

Discussion

The study in this paper reveals the benefit of the model-based integrated nonlinear approach to gas turbine engine sensor fault diagnostics in flight. Through this integrated architecture, the NBM is able to maintain its diagnostic effectiveness as the gas turbine engine health degrades over its lifetime. However, the integration of the two nonlinear models with different update strategies is not a trivial step. In this section, more detailed discussion and analysis about the integration are presented.

One issue that influences the integrated approach is the two-updated strategy involved in the health parameters calculation of the on-board engine model. If the health parameters of the on-board model are updated real time, the model estimated variables will track well the sensed measurements by the health parameters self-tuning no matter whether sensor failure happens. These model output values cannot be taken as the references to the sensed engine values. On the other hand, the model without performance update will be gradually away from the actual engine because of the engine health degradation with usage. Then, it is difficult to determine the abnormal caused by the modeling errors or sensor failures when the residual violates its threshold after operating several cycle numbers. It is desirable to draw out the advantages of the two model-based approaches with different performance update rate. In the case of the integrated architecture, the two performance update strategies are developed and combined to update the integrated models. The on-board adaptive model based on the EKF provides the unmeasured health parameters and tunes its performance real time, while the independent baseline model utilizes the soft update strategy to produce expected estimates of engine sensor measurements for the purposes of sensor fault diagnosis. These two on-board models used for the integrated architecture have different performance update periods in essence. Because the baseline model in the proposed architecture can track the actual engine well with usage, it is well suited for sensor fault diagnostics over time.

Another issue that influences the integrated approach is the application of the nonlinear model and the EKF algorithm. If the on-board adaptive model involves a linear model and piecewise LKF, such as the case for the bank of Kalman filter approach,[19] the modeling errors are inevitably produced in the model linearization process. Furthermore, the LKF algorithm design needs to be piecewise from the idle to the maximum operating condition for the gas turbine engine, and it increases the complexity to application.

Sensor fault threshold selection is also one of the important aspects to effectiveness of the sensor fault diagnosis. In order to make the system easy to detect the sensor fault with little amplitude changes, the threshold range needs to be set much smaller. In general, the fault threshold is obtained by the experiential data and is usually to be constant. In that case, no matter whether the model error changes, the threshold is always invariable. The model error will change with

the increased cycle number, and then the residual between the model and the actual engine is no longer the same as the initial cycle number under the scenarios of no sensor failure. The changed residual and the fixed threshold during the lifetime will unavoidably result in misdiagnosis. Therefore, a rational threshold selection is necessary for improving the accuracy of sensor fault diagnosis, and in the paper the model errors are taken into account to calculate the fault threshold.

In summary, the referred model accuracy and the fault threshold are the most important factors of the model-based approaches to sensor fault diagnosis. In this paper, the integrated architecture based on the nonlinear model is designed to improve the model accuracy, and the fault threshold is calculated by the statistical characteristics of sensor measurement noise and the model errors.

The problem of sensor fault diagnosis over the entire engine operating envelope also needs to be addressed. The proposed approach is mainly focused on the ground in the standard atmospheric pressure, and the experiments are carried out in this condition. A whole flight envelope approach to diagnose the sensor failure is necessary to engineering application, and optimal partitioning the whole envelope into regimes to correct the sensed parameters might be of significance to further study.

Conclusion

A model-based nonlinear integrated approach has been proposed to improve gas turbine engine sensor in-flight fault diagnostic accuracy over the course of engine lifetime. The designed architecture includes dual nonlinear on-board engine models and a sensor fault diagnostic module. The model with the two-update strategy is implemented to produce the baseline for the sensor fault diagnosis, and the sensor fault threshold is calculated by the modeling errors at the same time. Important theoretical and experimental results have been obtained on sensor fault diagnostics for turbofan engine. The theoretical results have also been validated by the experiment and analysis, which has shown good performance for both step fault and pulse fault to the sensor when the engine performance deteriorates with usage. The proposed method is easy to design and tuning with a promising potential application to gas turbine sensor fault diagnostics, due to its possibility to accommodate long-term engine health degradation.

Funding

This study was financially supported by the National Nature Science Foundation of China (No. 61304133), China Postdoctoral Science Foundation (No. 2013M530256), Jiangsu Province Nature Science Foundation (No. BK20130802), and Jiangsu Province Postdoctoral Science Foundation (No. 201202063).

Conflict of interest

None declared.

References

1. Garg S, Schadow K and Horn W. Sensor and actuator needs for more intelligent gas turbine engines. *NASA/TM-2010-216746*. Houston, TX: NASA, 2010.
2. Litt JS and Simon DL. *Towards a real-time measurement-based system for estimation of helicopter engine degradation due to compressor erosion. NASA/TM-2007-214843*. Virginia Beach, Virginia: NASA, 2007.
3. Hanumanthan H, Stitt A, Laskaridis P, et al. Severity estimation and effect of operational parameters for civil aircraft jet engines. *Proc IMechE, Part G: J Aerospace Engineering* 2012; 226: 1544–1561.
4. Delaat JC and Merrill WC. *Advanced detection isolation and accommodation of sensor failure in turbofan engine, real-time microcomputer implementation. NASA-90-2925*. Washington, DC: NASA, 1990.
5. Henriksson M, Gronstedt T and Breitholtz C. Model-based on-board turbofan thrust estimation. *Control Eng Pract* 2011; 19: 602–610.
6. Dimogianopoulos D, Hios J and Fassois S. Aircraft engine health management via stochastic modeling of flight data interrelations. *Aerosp Sci Technol* 2012; 16: 70–81.
7. Lei YG, Lin J, He ZJ, et al. A method based on multi-sensor data fusion for fault detection of planetary gearboxes. *Sensors* 2012; 12: 2005–2017.
8. Kurzke J. Sensor checking using model based engine performance test analysis and numerical optimization. In: *17th ISABE conference*, Munich, Germany 2005, paper no: ISABE-2005-1239. USA: ISABE.
9. Fast M. *Artificial neural networks for gas turbine modeling and sensor validation*. Master of Science Thesis, Lund University, Sweden, 2005.
10. Romesis C and Mathioudakis K. Setting up of a probabilistic neural network for sensor fault detection including operation with component faults. *J Eng Gas Turbines Power* 2003; 125: 634–641.
11. Wallhagen RE and Arpasi DJ. *Self-teaching digital computer program for fail operational control of a turbojet engine in a sea-level test stand. NASA/TM-X-3043*. Houston, TX: NASA, 1974.
12. Spang HA and Corley RC. Failure detection and correction for turbofan engine. In: *Proceedings of joint automatic control conference*, San Francisco, CA, USA, 22–24 June 1977, General Electronic Co. No.77CRD159.
13. Merrill WC, Delaat JC, Kroszkewicz SM, et al. Full-scale engine demonstration of an advanced sensor failure detection, isolation, and accommodation algorithm-preliminary results. In: *Guidance, Navigation, and Control Conference sponsored by the American Institute of Aeronautics and Astronautics*, Monterey, California, 17–19 August 1987, paper no. AIAA-87-2259. USA: AIAA.
14. Brown H and Vizzini RW. Analytical redundancy technology for engine reliability engine reliability improvement. SAE-861725, 1986.
15. Swan JA. *Analytical redundancy design for improved engine control reliability final review. AIAA-88-3776*. Houston, TX: NASA, 1988.

16. Bettocchi R and Spina PR. ARX linear model set up for fault diagnosis of gas turbine sensors. 2007, paper no. ASME Paper 97-GT-027. New York: ASME.
17. Simani S, Fantuzzi C and Beghelli S. Improved observer for sensor fault diagnosis for a power plant. In: *Proceedings of the 7th Mediterranean conference on control and automation*, Haifa, Israel, 28–30 June 1999.
18. Kobayashi T. *Aircraft engine sensor/actuator/component fault diagnosis using a bank of kalman filters. NASA/CR-2003-212298*. Houston, TX: NASA, 2003.
19. Ogaji SOT, Marinai L, Sampath S, et al. Gas-turbine fault diagnostics: a fuzzy-logic approach. *Appl Energy* 2005; 82: 81–89.
20. Mattern DL, Jaw LC and Guo TH. Simulation of an engine sensor validation scheme using an autoassociative neural network. In: *33rd Joint Propulsion Conference and Exhibit*, Seattle, WA, USA, 6–9 July 1997, paper no. AIAA-97-2902. USA: AIAA.
21. Mattern DL, Jaw LC and Guo TH. Using neural networks for sensor validation. In: *34th AIAA/ASME/SAE/ASEE Joint Propulsion Conference and Exhibit*, Cleveland, OH, USA, 13–15 July 1998, paper no. AIAA-98-3457. USA: AIAA.
22. Randal R, Daniel EV and Aditya K. Towards in-flight detection and accommodation of faults in aircraft engines. In: *Proceedings of AIAA 1st intelligent systems technical conference*, Chicago, IL, USA, 20–22 September 2004, AIAA-2004-6463.
23. Zhernakov SV. Diagnostics and checking of gas turbine engines parameters with hybrid expert systems. In: *Proceedings of workshop on computer science and information technologies CSIT,* Ufa*,* Russia, 15 March 2000, pp. 227–234.
24. Aretakis N, Mathioudakis K and Stamatis A. Identification of sensor fault on turbofan engines using pattern recognition techniques. *Control Eng Pract* 2004; 12: 827–836.
25. Tang L, Decastro JA, Zhang X, et al. A unified nonlinear adaptive approach for detection and isolation of engine faults. In: *Proceedings of ASME turbo expo 2010*, Glasgow, UK, 14–18 June 2010, NASA/TM-2010-216360.
26. Widodo A and Yang BS. Application of relevance vector machine and survival probability to machine degradation assessment. *Expert Syst Appl* 2010; 28: 2592–2599.
27. Lu F, Huang J and Xing Y. Fault diagnostics for turboshaft engine sensors based on a simplified on-board model. *Sensors* 2012; 12: 11061–11076.
28. Kyprianidis KG, Sethi V, Ogaji SOT, et al. Uncertainty in gas turbine thermo-fluid modeling and its impact on performance calculations and emissions predictions at aircraft system level. *Proc IMechE, Part G: J Aerospace Engineering* 2012; 226: 163–181.
29. Doel DL. TEMPER – a gas path analysis tool for commercial jet engines. *J Eng Gas Turbines Power* 1994; 116: 82–89.
30. Mathioudakis K, Kamboukos P and Stamatis A. Turbofan performance deterioration tracking using nonlinear models and optimization techniques. ASME paper GT-2002-30026, 2002.
31. Kobayashi T and Simon DL. Integration of on-line and off-line diagnostic algorithms for aircraft engine health management. In: *Turbo Expo 2007 sponsored by the American Society of Mechanical Engineers*, Montreal, Canada, May 14–17 2007, paper no. NASA/TM-2007-214980. USA: NASA.
32. Kobayashi T and Simon DL. Aircraft engine on-line diagnostics through dual-channel sensor measurements: Development of a baseline system. In: *Proceedings of ASME turbo expo 2008 gas turbine congress and exposition*, Berlin, Germany, 9–13 June 2008, NASA/TM-2008-215228.
33. Kobayashi T and Simon DL. Aircraft engine on-line diagnostics through dual-channel sensor measurements: development of an enhanced system. In: *Proceedings of ASME turbo expo 2008*, Berlin, Germany, 9–13 June 2008, paper no. NASA/TM-2008-215229. Berlin, Germany: NASA.
34. Simon DL. An integrated architecture for on-board aircraft engine performance trend monitoring and gas path fault diagnostics. In: *57th Joint Army-Navy-NASA-Air Force (JANNAF) Propulsion Meeting sponsored by the JANNAF Interagency Propulsion Committee*, Colorado Springs, Colorado, May 3–7 2010, paper no. NASA/TM-2010-216358. USA: NASA.
35. Armstrong JB and Simon DL. Implementation of an integrated on-board aircraft engine diagnostic architecture. In: *47th Joint Propulsion Conference and Exhibit cosponsored by the AIAA, ASME, SAE, and ASEE*, San Diego, California, July 31–August 3 2011, paper no. AIAA–2011–5859. USA: AIAA/NASA.
36. Simon D. A comparison of filtering approaches for aircraft engine health estimation. *Aerosp Sci Technol* 2008; 12: 276–284.
37. Julier S, Uhlmann J and Durrant-Whyte H. A new method for the nonlinear transformation of means and covariances in filters and estimators. *IEEE Trans Automat Control* 2000; 45: 477–482.
38. Sun JG, Vasilyev V and Ilyasov B. *Advanced multivariable control systems of aeroengines*. Beijing: Beihang Press, 2005.
39. Lu F. *Aero-engine fault diagnostics based on fusion technique*. PhD Thesis, Nanjing University of Aeronautics and Astronautics, Nanjing, 2009.
40. The Research and Technology Organization of NATO. Performance prediction and simulation of gas turbine engine operation for aircraft, marine, vehicular, and power generation. RTO-TR-AVT-036, 2007.
41. Simon DL. Propulsion diagnostic method evaluation strategy (ProDiMES) user's guide. NASA Technical Report. Report no. NASA/TM-2010-215840, 1 January 2010. Cleveland, Ohio: NASA.
42. Lu F, Huang J and Lv Y. Gas path health monitoring for a turbofan engine based on nonlinear filtering approach. *Energies* 2013; 6: 492–511.
43. Jaw LC and Wang W. Mathematical formulation of model-based methods for diagnostics and prognostics. In: *ASME Turbo Expo 2006: Power for Land, Sea and Air*, Barcelona, Spain, 2006, paper no: GT-2006-90655, pp.691–697. New York: ASME.